Lithospheric velocity structure of the Anatolian plateau-Caucasus-Caspian region

R. Gök,[1] R. J. Mellors,[2,3] E. Sandvol,[4] M. Pasyanos,[1] T. Hauk,[1] R. Takedatsu,[2] G. Yetirmishli,[5] U. Teoman,[6] N. Turkelli,[6] T. Godoladze,[7] and Z. Javakishvirli[7]

Received 30 December 2009; revised 26 January 2011; accepted 1 February 2011; published 7 May 2011.

[1] The Anatolian plateau-Caucasus-Caspian region is an area of complex lithospheric structure accompanied by large variations in seismic wave velocities. Despite the complexity of the region, little is known about the detailed lithospheric structure. Using data from 31 new, permanent broadband seismic stations along with results from a previous 29 temporary seismic stations and 3 existing global seismic stations in the region, a 3-D velocity model is developed using joint inversion of teleseismic receiver functions and surface waves. Both group and phase dispersion curves (Love and Rayleigh) were derived from regional and teleseismic events. Additional Rayleigh wave group dispersion curves were determined using ambient noise correlation. Receiver functions were calculated using *P* arrivals from 789 teleseismic (30°–90°) earthquakes. The stacked receiver functions and surface wave dispersion curves were jointly inverted to yield the absolute shear wave velocity to a depth of 100 km at each station. The depths of major discontinuities (sediment-basement, crust-mantle, and lithosphere-asthenosphere) were inferred from the velocity-depth profiles at the location of each station. Distinct spatial variations in crustal and upper mantle shear velocities were observed. The Kura basin showed slow (~2.7–2.9 km/s) upper crustal (0–11 km) velocities but elevated (~3.8–3.9 km/s) velocities in the lower crust. The Anatolian plateau varied from ~3.1–3.2 in the upper crust to ~3.5–3.7 in the lower crust, while velocities in the Arabian plate (south of the Bitlis suture) were slightly faster (upper crust between 3.3 and 3.4 km/s and lower crust between 3.8 and 3.9 km/s). The depth of the Moho, which was estimated from the shear velocity profiles, was 35 km in the Arabian plate and increased northward to 54 km at the southern edge of the Greater Caucasus. Moho depths in the Kura and at the edge of the Caspian showed more spatial variability but ranged between 35 and 45 km. Upper mantle velocities were slow under the Anatolian plateau but increased to the south under the Arabian plate and to the east (4.3–4.4 km/s) under the Kura basin and Greater Caucasus. The areas of slow mantle coincided with the locations of Holocene volcanoes. Differences between Rayleigh and Love dispersions at long wavelengths reveal a pronounced variation in anisotropy between the Anatolian plateau and the Kura basin.

Citation: Gök, R., et al. (2011), Lithospheric velocity structure of the Anatolian plateau-Caucasus-Caspian region, *J. Geophys. Res.*, *116*, B05303, doi:10.1029/2009JB000837.

1. Introduction

[2] The continental collision zone between the Arabian and Eurasian plates has led to formation of a 2 km high plateau and the formation of a diffuse zone of deformation that extends from the Bitlis suture to the Greater Caucasus (Figure 1). In addition to the fold and thrust belts typical of most continental collision zones, the Arabia-Eurasia transition zone includes the South Caspian Basin, a 20 km deep sedimentary basin of uncertain origin [*Sengör*, 1990; *Brunet et al.*, 2003; *Khain*, 2005] and the Anatolian plateau, an uplifted volcanic area with active faulting [*Barazangi et al.*, 2006; *Göğüş and Pysklywec*, 2008; *Ershov and Nikishin*, 2004; *Maggi and Priestley*, 2005]. Explanations of this diversity in tectonic styles differ but generally invoke subduction (and/or

[1]Lawrence Livermore National Laboratory, Livermore, California, USA.
[2]Department of Geological Sciences, San Diego State University, San Diego, California, USA.
[3]Now at Lawrence Livermore National Laboratory, Livermore, California, USA.
[4]Department of Geological Sciences, University of Missouri, Columbia, Missouri, USA.
[5]Republic Seismic Survey Center, Baku, Azerbaijan.
[6]Kandilli Observatory and Earthquake Research Institute, Department of Geophysics, Bogazici University, Istanbul, Turkey.
[7]Earth Research Institute, Ilia State University, Tbilisi, Georgia.

0148-0227/11/2009JB000837

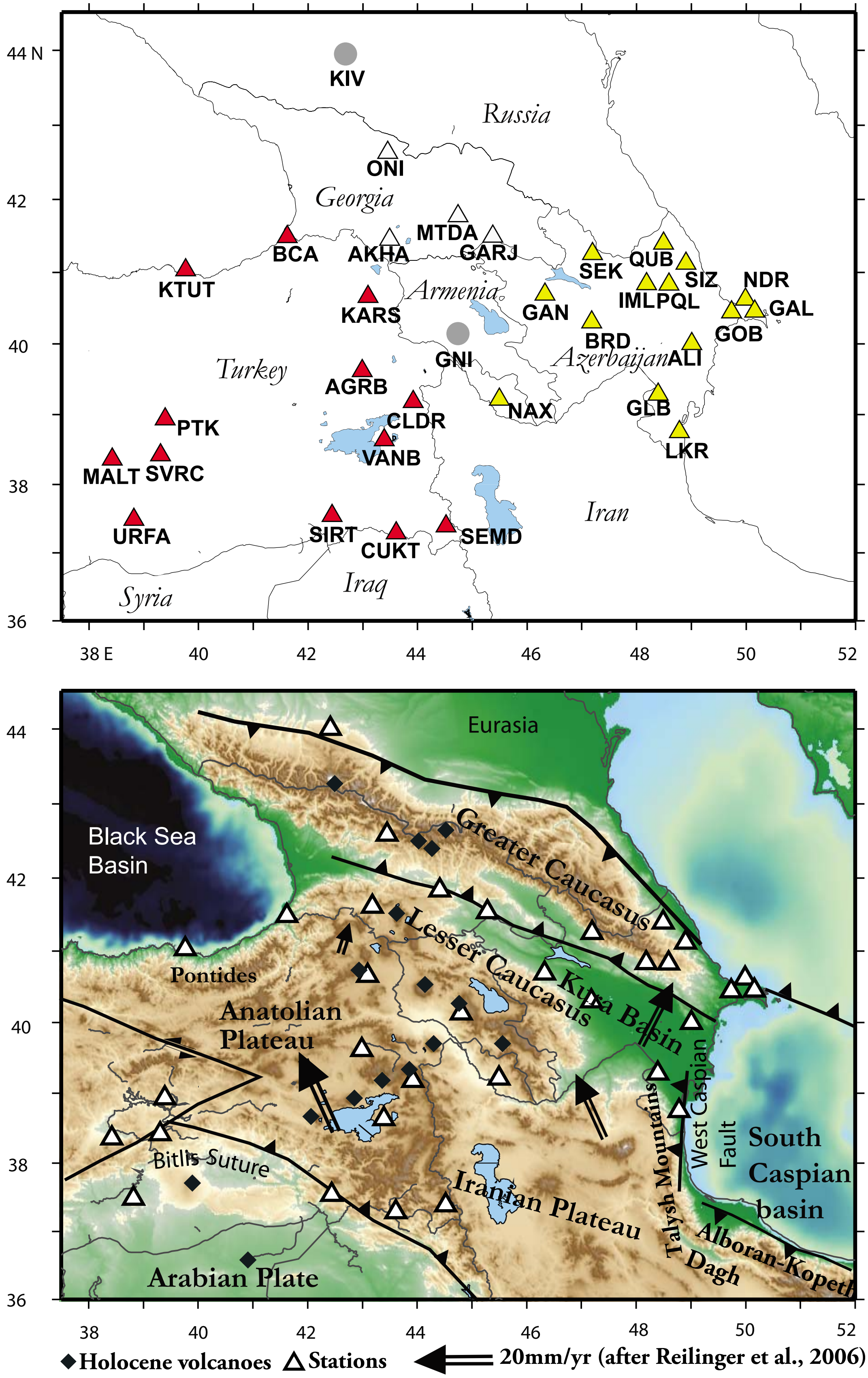

Figure 1. (top) Stations that contributed data to this study. Stations are color-coded by country (Turkey, red; Georgia, white; Azerbaijan, yellow; Global Seismographic Network stations, gray circles). (bottom) Tectonic features of stations in Figure 1 (top).

delamination) episodes embedded within the collision zone [*Priestley et al.*, 1994; *Sengör et al.*, 2003; *Masson et al.*, 2006; *Göğüş and Pysklywec*, 2008]. Contributing to the poor understanding is the lack of a comprehensive crustal and lithospheric velocity model of the region. Large-scale regional and global models [e.g., *Bijwaard et al.*, 1998; *Piromallo and Morelli*, 2003] show intriguing velocity variations in the upper mantle but cannot resolve the fine details. In the Caucasus region much of the detailed information on crustal and upper mantle velocity structure is based on refraction data collected in the 1960s [e.g., *Kondorskaya et al.*, 1981] along with data from a few temporary deployments and sparse global seismic stations [*Mangino and Priestley*, 1998]. More recent data [e.g., *Sandvol et al.*, 2003] collected in the Anatolian plateau have imaged the bulk lithospheric structure of eastern Anatolia but the transitions between the plateau and the surrounding tectonic units are unclear. A comprehensive velocity model would aid in the understanding of this complex region. A detailed model is also essential in mapping regional wave propagation and improving the accuracy of earthquake hypocenters throughout the region.

[3] This paper presents a model of the crustal and upper mantle structure of the Anatolian plateau-Caucasus-Caspian region using waveform data from 31 new broadband stations in the region (Figure 1) combined with previous data. The new broadband stations are part of the Azerbaijan, Georgian, and Turkish national seismic networks. The spatial coverage of this data set represents a significant improvement over previously available broadband data, which were restricted to three global stations and a few temporary deployments. In this study, we combine surface waves with receiver functions to obtain a constrained shear wave velocity model of the crust and upper mantle to a depth of 100 km. The results provide a comprehensive view of the crustal structure and illuminate the transitions between the various tectonic units. This paper is primarily focused on presenting the lithospheric seismic velocity structure and the regional wave propagation as determined from this study rather than a detailed tectonic interpretation. However, we provide a brief overview of the regional setting and some unresolved questions of this intriguing region below.

2. Geologic and Tectonic Setting

[4] A broad zone of deformation exists along the northern edge of the Arabian plate and extends from the Zagros Mountains to the Caucasus-Caspian region. The current style of deformation varies from compression and thrusting in the Zagros to strike slip in the Anatolian plateau [*Allen et al.*, 2004]. As the Arabian plate is moving northward with respect to Eurasia at a rate of approximately 18 mm/yr [*Reilinger et al.*, 2006], the deformation zone has generally been attributed to the ongoing continental collision [*Dewey and Şengör*, 1979] but other mechanisms such as orogenic collapse or slab pull may play a significant role [*Allen et al.*, 2004; *Vernant and Chery*, 2006]. Prior to the present configuration, active subduction of the Neo-Tethys oceanic lithosphere occurred along the northern edge of the Arabian plate. This subduction ceased approximately 24 Ma at the beginning of the Miocene as all oceanic crust was consumed [*Sengör et al.*, 2003] although the timing varies substantially along the Eurasian-Arabian plate boundary. The continued Arabian-Eurasia convergence has affected the Anatolian plateau and the Lesser and Greater Caucasus in distinctly different fashions.

[5] The Anatolian plateau is an uplifted volcanic plateau [*Barazangi et al.*, 2006; *Maggi and Priestley*, 2005] with an average crustal thickness of 40–50 km that increases from south to north. Low *Pn* velocities (7.6 km/s), highly attenuated *Sn*, and receiver functions indicate that the lithospheric mantle is thin or missing [*Gök et al.*, 2003; *Zor et al.*, 2003; *Al-Lazki et al.*, 2004; *Angus et al.*, 2006] and therefore elevations are supported by buoyant asthenosphere rather than thickened crust [*Sengör et al.*, 2003]. The abnormally hot upper mantle and widespread volcanics may be related to the detachment of the subducting slab or continental delamination about 11 Ma. Detailed receiver functions and resistivity measurements indicate that the possible delaminated lithospheric fragments possess a complex geometry [*Ozacar et al.*, 2008; *Türkoğlu et al.*, 2008]. An alternate possibility is that remnant water and fluids from the subducting oceanic slab may be affecting mantle properties [*Hearn and Ni*, 1994; *Maggi and Priestley*, 2005], although the chemistry of the volcanic rocks is not consistent with this interpretation.

[6] North of the Anatolian plateau and between the South Caspian and the Black Sea lies a complex area containing the Lesser and Greater Caucasus which are separated on the eastern side by the Kura basin. Remarkably, the Lesser Caucasus includes strike-slip, compressional and extensional structures as well as significant volcanism. The variety of faulting is apparently due to east-west extension caused by the westward movement of the Anatolian plate away from the north-south compression within the Arabian-Eurasian collision zone [e.g., *Rebai et al.*, 1993].

[7] North of the Lesser Caucasus and bordering the South Caspian Basin is the Kura basin, a lowland with up to 15 km of sediments [*Brunet et al.*, 2003] and inferred to be a foreland basin to both the Greater and Lesser Caucasus. Structurally, it is separated from the South Caspian Basin by a ridge of uplifted basement (the Talysh-Vandam basement high) and the inferred West Caspian fault [*Kadirov and Askerhanova*, 1998] although the exact nature of the transition between the South Caspian and the Kura basin remains uncertain. Refraction data indicate a high-velocity lower crust [*Kondorskaya et al.*, 1981]. The Kura basin is bordered on the southeast by the thrust faults of the Talysh Mountains and on the southwest by the Lesser Caucasus. Regional wave propagation and velocities are poorly constrained in this region but it appears that high *Pn* and *Sn* velocities extend into the Kura basin from the South Caspian but that *Sn* may be attenuated in the western Greater Caucasus [*Martin et al.*, 2005].

[8] The Greater Caucasus is primarily a fold and thrust belt and represent the northern extent of significant deformation between the Arabian and Eurasian plates. GPS data show about 7 to 14 mm/yr of shortening across the Greater Caucasus [*Reilinger et al.*, 2006; *Masson et al.*, 2006]. This, along with a few apparently deep earthquakes, has been interpreted to suggest that subduction may be continuing under the Greater Caucasus [*Khain and Lobkovskiy*, 1994; *Vernant and Chery*, 2006]. The western Greater Caucasus includes several Holocene volcanic areas, and gravity data indicate a decrease in lithospheric strength from east to west [*Ruppel and McNutt*, 1990]. *Sn* also appears to suffer greater attenuation in the western Caucasus than in the eastern

section [*Gök et al.*, 2003]. Refraction data indicate a crustal thickness of approximately 50–55 km with moderate to low crustal velocities [*Ershov and Nikishin*, 2003].

[9] Adjacent to our study area but of great interest is the South Caspian Basin, a deep (~20 km) sedimentary basin filled with mostly Pliocene-Quaternary sediments [*Knapp et al.*, 2004; *Allen et al.*, 2002; *Brunet et al.*, 2003]. The exact origin and age of the South Caspian remains uncertain and it may be remnant oceanic crust [*Nadirov et al.*, 1997], a large-scale pull-apart basin [*Sengör*, 1990], or a back-arc basin which underwent increased subsidence at the onset of continental collision [*Brunet et al.*, 2003]. The northern edge is marked by a large anticline, the Absheron megastructure, which coincides with a northwest-southeast belt of seismicity including moderate depth (as deep as 80 km) earthquakes that occur at the northern edge of the South Caspian Sea basin. This seismicity [*Jackson et al.*, 2002] as well as gravity [*Allen et al.*, 2002] and deep seismic reflection data [*Knapp et al.*, 2004] suggest that the South Caspian crust is subducting northward under the Eurasia plate along this zone. It is unclear if and how far the subduction extends to the west. *Lg* is blocked but *Sn* propagates well [*Kadinsky-Cade et al.*, 1981; *Rodgers et al.*, 1997; *Gök et al.*, 2003]. *Pn* velocities are normal or possibly slightly elevated (e.g., 8.0–8.2 km/s) [*Hearn and Ni*, 1994; *Al-Lazki et al.*, 2003; *Toksöz et al.*, 2006].

[10] In general, while a variety of studies on the seismic velocity structure of each unit have been conducted a comprehensive high-resolution model that includes the transitions zones as well as the individual units is lacking. This paper seeks to provide a clear and comprehensive seismic model of this area that will be useful for understanding and modeling regional wave propagation as well as the underlying tectonics.

3. Data

[11] Recently, permanent broadband stations have been deployed across the Caucasus and eastern Turkey region as part of various national networks (Azerbaijan (14), Georgia (4), and Turkey (13)) providing an excellent opportunity to study the lithospheric structure. We used data from 31 newly available broadband stations that have been installed in recent years (Figure 1). These stations are part of the Azerbaijan National Seismic network, the Georgian Seismic Network, and stations run by Kandilli Observatory in Turkey. The Azeri stations use STS-2 seismometers and the Kandilli and Georgian network include a mix of CMG-3ESP, CMG-3T and CMG-40T instruments. To accompany this data set, waveform data were also collected from 2005 to 2009 for the relevant Global Seismographic Network (GSN) stations (GNI, ABKT, and KIV). Considerable effort was made in evaluating and testing the available instrument responses for each station. The calibration was conducted by removing the instrument response and then comparing waveforms of events among stations and with a modeled event.

4. Method

[12] The combination of receiver functions and surface waves is a powerful method to infer crustal and upper mantle shear wave velocities. Receiver functions isolate the response of near vertically propagating plane waves to seismic velocity discontinuities under a seismic station and are primarily sensitive to the depth of velocity contrasts but have poor sensitivity to absolute velocities. Surface wave dispersion is primarily controlled by the *S* wave velocity structure but possesses poor sensitivity to velocity discontinuities or fine structure. Therefore, inverting both surface wave dispersion and receiver functions simultaneously should improve the reliability of the results [*Julia et al.*, 2000].

4.1. Receiver Functions

[13] Teleseismic events between 30° and 90° with a magnitude greater than $m_b = 5.5$ were extracted from the data and receiver functions were calculated for all stations. Owing to varying data availability, the largest number of events was recorded by the GSN stations with over 600 candidate events. Most of the other stations possessed between 100 and 200 candidate events. Azimuthal coverage was excellent to the east but poorer toward the west (Figure 2). Teleseismic waveforms were decimated at 20 SPS, and windowed between 40 s prior and 60 s after the *P* onset time. The data were demeaned and detrended and a taper was applied prior to the deconvolution. Traces were rotated to great circle path on horizontals. The time domain iterative deconvolution of *Ligorria and Ammon* [1999] with 100 iterations was used to calculate the receiver functions with a Gaussian filter (*a*, the filter width parameter) of 1.0, 1.5, and 2.5. The large variations (such as Moho) should be more prominent on smaller Gaussian width (1.0) filtered traces whereas high-frequency (2.5) receiver functions would be more sensitive to thinner layering within the crust. All events and receiver functions were visually inspected for high signal to noise and only results with a high signal-to-noise ratio were used.

[14] The quality of the receiver functions was poor for several of the Azerbaijan stations owing to high noise levels (especially NDR, GOB, and GAL). Thick sedimentary layers produced pronounced multiples under most stations. Figure 2 shows the radial component receiver functions for all events at selected, characteristic stations plotted as a function of back azimuth. Because of the limited space here we will be discussing only these selected stations. Very strong crustal reverberations are observed at stations BRD, QUB and IML. LKR, located at the boundary between Talysh Mountains and the Kura basin, displays a clear consistent Ps_{MOHO}. Variations in receiver functions waveforms with back azimuth and significant energy on the tangential components suggest important lateral variations in structure under several stations as well (e.g., QUB, MTDA, and LKR in Figure 2). As most of the seismic sources are located to the east, detailed variations in receiver functions with back azimuth cannot be resolved. In general, the stations in eastern Turkey showed clearer results although CUKT, located at the Bitlis suture, has a slightly noisier and incoherent signal combined with low-amplitude Ps_{MOHO}. We initially used forward modeling and the slant stack technique of *Zhu and Kanamori* [2000] to estimate Moho depth and crustal properties. However, shallow low velocities/sedimentary basin caused reverberations in the receiver functions which added considerable uncertainty to the estimates. Supporting evidence for these low velocities can be found from a deep (~8 km) borehole (Saatly) drilled in the Kura basin on a "basement high" [*Kadirov and Askerhanova*, 1998]. It is approximately halfway between stations ALI and BRD. The borehole revealed

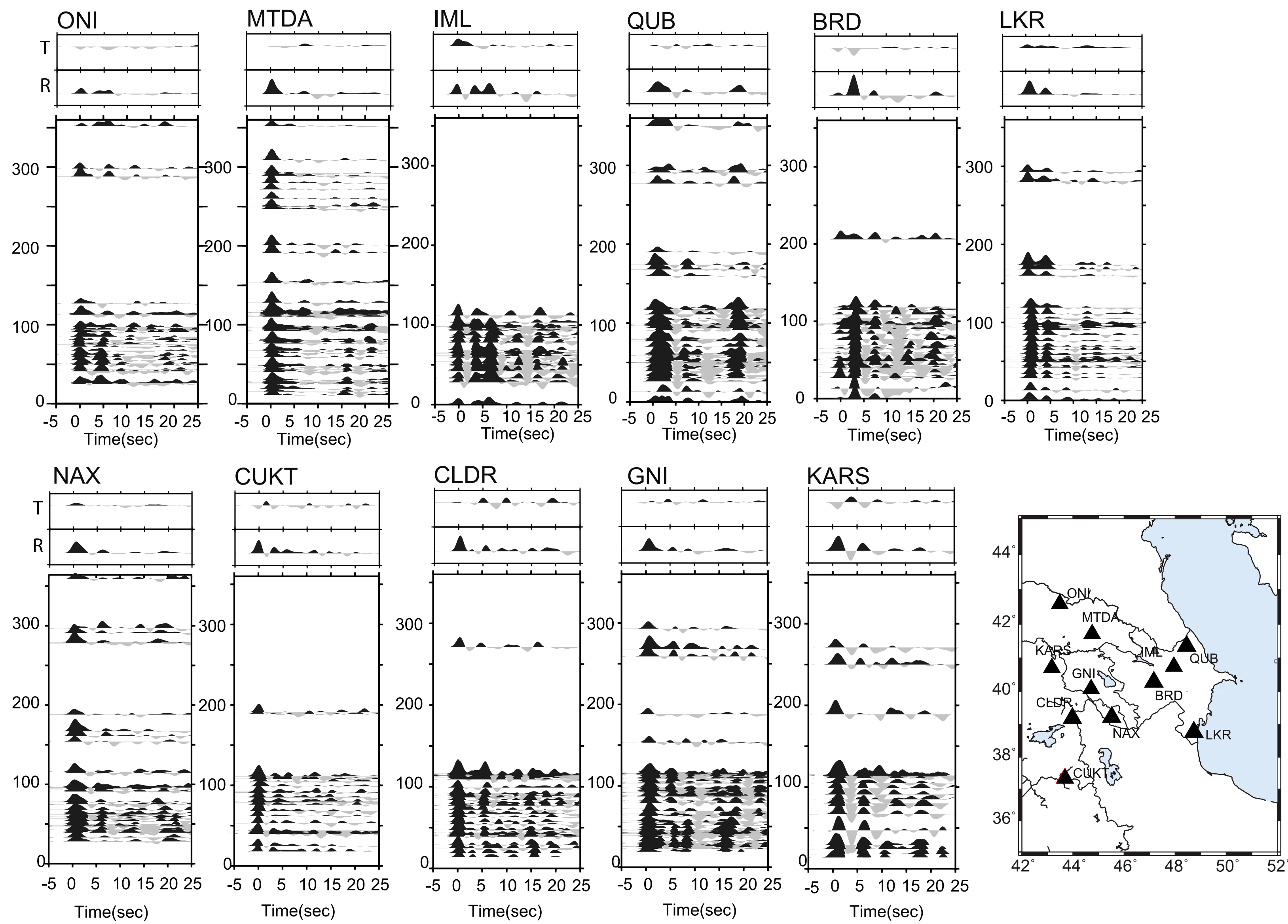

Figure 2. Radial receiver functions (filtered with a Gaussian filter width of 1.0 s) plotted as a function of back azimuth from selected stations in the region. The stacked traces of radial (R) and transverse (T) receiver functions are shown on top of each plot.

a complex interlaying of sedimentary rock (clastic and carbonate) with volcanoclastics which graded gradually into a more volcanic sequence at the bottom.

[15] We prefer using the results provided by the joint inversion as we consider them more robust. We stacked the receiver functions on the basis of the coherency of the waveforms since we are not seeking to resolve the azimuthal dependence within the scope of this paper.

4.2. Surface Wave Analysis

[16] Several methods were used to obtain surface wave dispersion curves. These included event-based methods used for both group and phase velocities as well as Rayleigh wave group velocity dispersion estimate from ambient noise cross correlation [e.g., *Shapiro and Campillo*, 2004].

[17] We calculated the Love and Rayleigh wave group velocity dispersion curves of over 1500 waveforms (7–90 s) at distances of 0–90°. Waveforms were detrended, filtered, decimated to 1 SPS and dispersion curves were manually picked using a multiple frequency implementation [*Herrmann*, 1973]. The horizontal components showed higher noise levels than the vertical component and hence the dispersion curves for Love waves have higher errors than the corresponding Rayleigh dispersion curves especially at longer (more than 70 s) periods. Ambient noise correlation was applied to 406 station pairs to obtain Rayleigh wave group velocities [*Shapiro and Campillo*, 2004; *Bensen et al.*, 2007]. Data were corrected for the instrument response, band-pass-filtered, demeaned, detrended, whitened and sign-bit-normalized prior to the correlation. Figure 3a shows the Green's functions obtained by cross-correlating 1 h segments of vertical component data from station GNI with all other stations, stacking, and then filtering at 20–50 s. Again, owing to variation in available data, the amount of interstation overlap varied but the shortest period of interstation overlap was 90 days.

[18] Group velocity dispersion curves from all station-event and station-station (ambient noise) correlations were inverted using the surface wave tomography algorithm of *Pasyanos* [2005]. The inversion also includes measurements from other stations in the region (see Figure 3b for the ray density map). This method generates interpolated dispersion curves over a set of spatial grid points (0.5° × 0.5°). The Rayleigh and Love group velocity dispersion curves appropriate for each station were then extracted from the tomographic inversion. Results from three stations (in the Kura basin, Anatolian plateau, and Greater Caucasus) are shown in Figure 3b. Velocities in the Anatolian plateau are significantly lower at longer periods, whereas velocities in the Kura and Greater Caucasus are low at short periods where crust is overlain by thick sediments.

[19] The phase velocity map was obtained with the method of *Yang and Forsyth* [2006]. Data from an earlier temporary deployment of 29 stations were used as well as the newer data. Teleseismic earthquakes with a magnitude greater than 5.8 were selected and the waveforms were evaluated for high signal to noise at the longer periods (50 and 125 s). Unfortunately, many of the Azerbaijan stations showed high noise levels at the longer periods even on the vertical component, possibly owing to barometric variations. This restricted the data set to fewer events. The data for each event were decimated, filtered to create 13 frequency bands with corresponding centered periods ranging from 20 to 145 s and dispersion curves were estimated from these results. Initially, the Rayleigh wave phase dispersion was inverted to estimate 1-D velocities. The results were tomographically inverted for 2-D structure on a 50 km grid. *Yang and Forsyth* [2006] technique attempts to compensate for scattering caused by local heterogeneities and therefore should improve spatial resolution. The results at shorter wavelengths were more robust than for the longer wavelengths especially for the area covered by the Azeri stations, possibly owing to excessive noise at longer wavelengths. Higher upper mantle velocities were observed under Anatolia and lower velocities under the Caucasus-Caspian [*Skobeltsyn et al.*, 2009]. The phase velocity dispersion curves for each station were extracted from the tomography maps of *Skobeltsyn et al.* [2009].

[20] Inspection of the phase and group velocity maps showed trends consistent with the known surface geology. Compared to Kura and Greater Caucasus, we observe lower group velocities below the eastern Anatolian plateau above 45 s. Highest velocities in the upper mantle are observed in the Greater Caucasus, while the slowest velocities at short periods (10–30 s) are observed both Greater Caucasus and Kura basin which reflects the slow, thick sediments of the region.

5. Joint Inversion

[21] The stacked radial receiver functions (Gaussian filtered at 1.0, 1.5, and 2.5) and the interpolated dispersion curves (Rayleigh (group and phase), Love (group)) for each station are inverted to yield a 1-D shear wave model to a depth of 100 km at each station location. The method of *Julia et al.* [2000] is used. In brief, an iterative, damped, least squares algorithm is applied to find the best fitting model that fits both the observed receiver functions and the dispersion curves. Important adjustable parameters are the starting model, the smoothing between adjacent vertical layers, and the relative weighting between the data sets (receiver functions and surface waves). Additional details can be found in the work of *Julia et al.* [2000, 2003], and the reader is advised to consult those for further details.

[22] Initially, a simplified continental model was used based on the combined IASPEI91 and AK135 global models. For stations in the Kura basin region the inversion did not converge and a thick, low-velocity sedimentary layer was added to the starting model in accordance with the known structure of the region based on deep drill holes, surface geology, and a geophysical studies [e.g., *Kadirov and Askerhanova*, 1998]. We replaced the uppermost crustal layer with 10 km of low-velocity, sedimentary layer (Figure 4, blue line). The initial model used for the inversion consisted of constant velocity layers that increase in thickness with depth. Layer thicknesses were 2 km between 0 and 16, 3 km between 16 km and 60 km, and 4–25 km between 6 and 150 km. Note that inversion is performed down to 150 km but we present only 100 km for this paper as we believe the upper section is better constrained. Three different weighting schemes were tested (30%/70%, 50%/50%, and 70%/30%) to weight the receiver function and surface wave misfit, respectively. We fixed the smoothness parameter [*Julia et al.*, 2000, equation (6)] to 0.6 during inversion. We found that 0.6 would converge without losing much of the detailed structure.

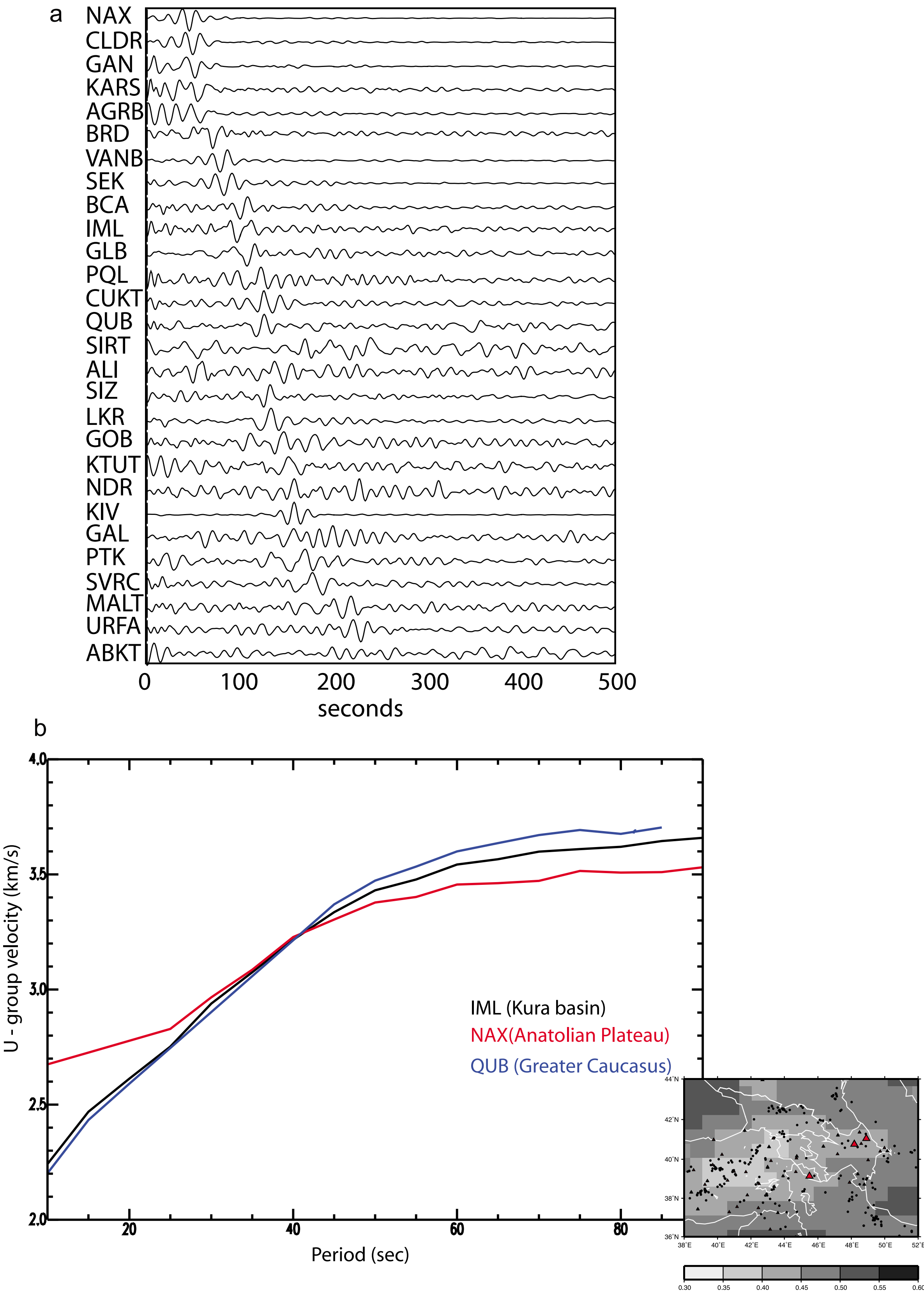

Figure 3. (a) Ambient noise correlation results of station GNI with the rest of stations, filtered at 20–50 s and sorted by distance. (b) Example of surface wave group velocity dispersion curves extracted from the regional/global tomography map after including data from this study. Inset is the ray density map (with highlighted station locations shown on the graph).

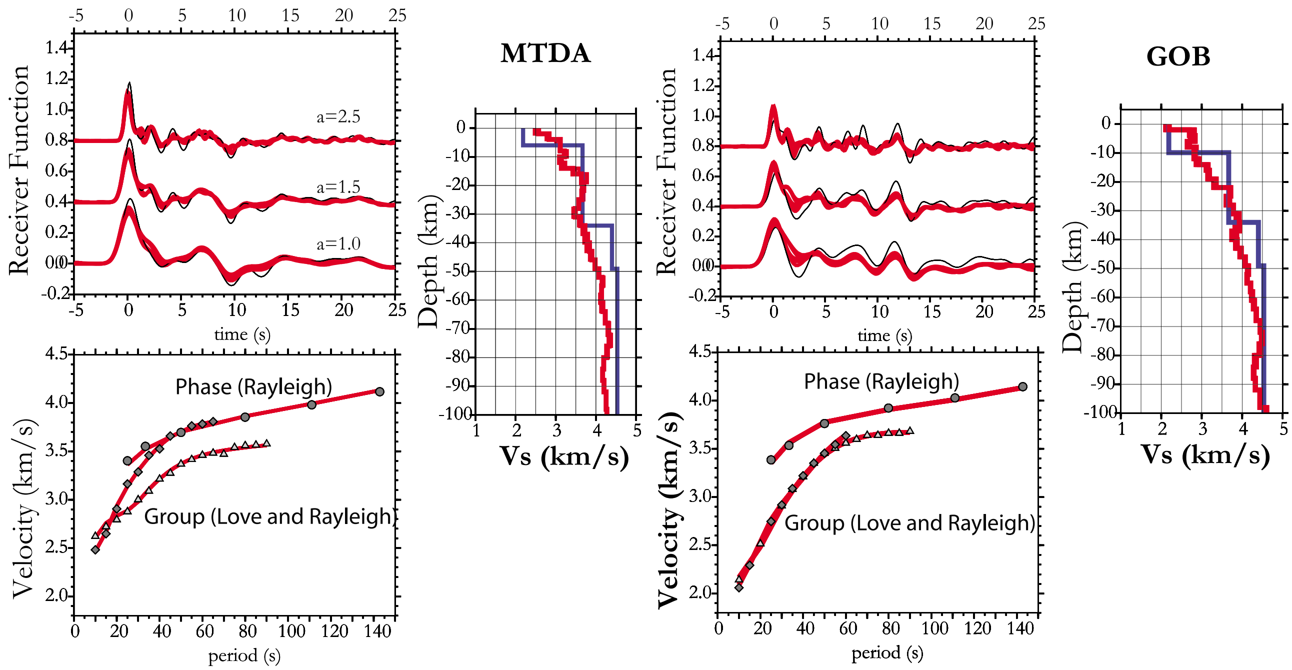

Figure 4. Two examples of how the joint inversion is performed with combined measurements. Note that the Love and Rayleigh waves completely overlap between 10 and 50 s for station GOB in Kura basin. The blue line is the starting model for each station. The red line is synthetic.

[23] In most cases, velocity profiles for all three relative weights were similar except at shallow (<10 km) depths. Figure 4 shows two examples of the joint inversion data and results for station MTDA and GOB. MTDA is located between the Lesser and Greater Caucasus whereas GOB is on thick sediments of the Absheron peninsula at the edge of the South Caspian Basin. A 1-D velocity profile was obtained for each station and examples are shown in the Figure 4. There were cases where it was difficult to fit both Love and Rayleigh waves. Love waves are sensitive to the velocity of horizontally propagating SH waves while the receiver functions and Rayleigh waves are sensitive to the vertically propagating SV waves. The inability to fit data in the long-period portion of the dispersion curves may indicate the existence of radial anisotropy in the upper mantle.

[24] As a result, we tested several methodologies to obtain the best fit to the observed receiver functions and dispersion curves with the existing algorithm, which assumes an isotropic model. As noted above, the difficulty in fitting both Love and Rayleigh occurred in the upper mantle; resolution of crustal layers was unaffected. The preferred procedure initially inverted the Rayleigh phase and group dispersion jointly with the receiver functions to yield a Rayleigh/receiver function model. The Rayleigh/receiver function was then used as a starting model for a Love wave/receiver function inversion. This yielded two similar models that differed slightly (usually <5%) but systematically in the upper mantle. These two models were averaged together to produce a final velocity profile at each station and provided a good fit to the receiver functions. As a test of robustness, this procedure was run using the three different weighting schemes described above and converged to a similar profile for each case. Independent inversions using Love and Rayleigh waves separately were also performed.

6. Results and Discussion

[25] Inversion results are shown in Figures 5 and 6. We combined the 34 (31 new measurements plus 3 GSN stations ABKT, KIV and GNI) with results from a previous 29 station temporary deployment on the Anatolian plateau processed using similar methods (joint inversion of receiver functions and surface waves) from *Gök et al.* [2007].

[26] Moho depths were estimated from the shear wave profiles by visually inspecting profiles for large gradient change and a threshold value of 4.2 km/s, which was chosen as a consistently lowest bound for the upper mantle velocity values in the region. After inspecting 1-D profiles we feel that this cutoff value would represent the depth of Moho where it is smoothed by either inversion or surface waves or receiver function amplitudes. Figure 5 shows the resulting map derived by interpolating the Moho depth estimates at each station using a nearest-neighbor gridding algorithm [*Wessel and Smith*, 1998]. The Lesser Caucasus has the thickest crust (~52 km), which is thinner than the estimate of *Sandvol et al.* [1998], which was based on a single station (GNI) receiver function inversion using far less data than this study. Coverage of the Greater Caucasus was sparse, but suggests 50 km in the west and 45–50 in the east. The Kura-South Caspian transition zone showed mixed results, possibly owing to poor resolution by the receiver functions related to multiples within the upper crust and high noise levels at stations on the Absheron Peninsula. In general, the crust thins toward the South Caspian Basin. The Arabian

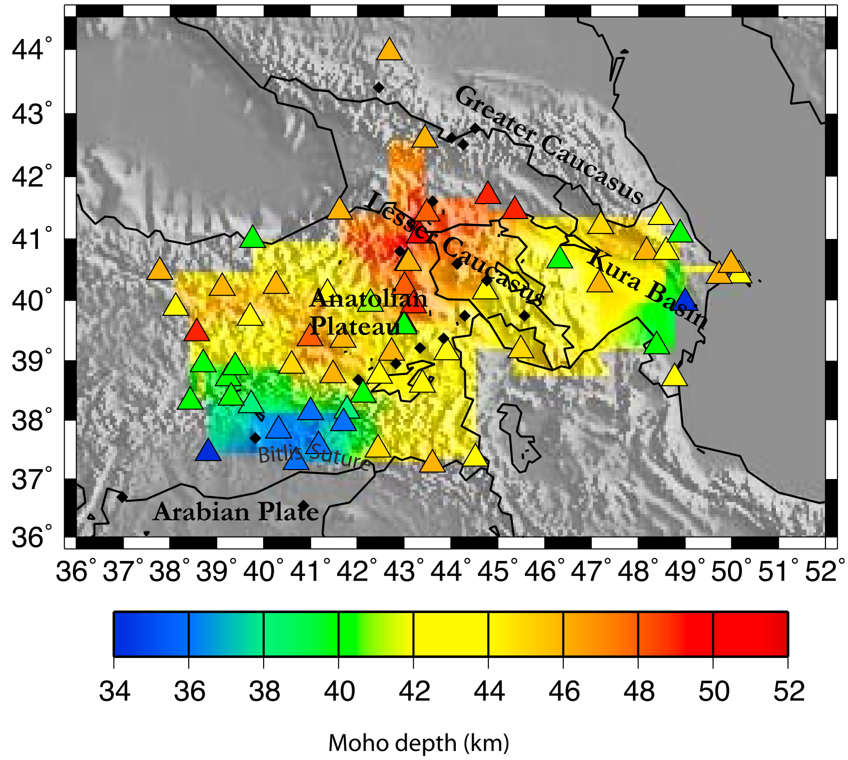

Figure 5. Interpolated Moho depths of this study including Moho depth results from the Eastern Turkey Seismic Experiment (ETSE) network [*Gök et al.*, 2003]. The deepest Moho is observed in the Lesser Caucasus region, and the shallowest is in the Arabian plate.

plate showed the most homogenous results with thickness of 35 km.

[27] The absolute velocities in Figure 6 are the result of averaged Rayleigh/receiver function and Love/receiver function output models with receiver function inversion at 10, 35 and 85 km are shown in Figure 6. The thick sediments of Kura basin is still observed with low velocities with the average Vs = 2.8 km/s at 10 km slice. The eastern part of the Greater Caucasus shows similar low velocities in the upper crust. The northern part of mountains is also overlain by relatively young Oligocene to Quaternary sediments. The slowest lower crustal velocities are observed in the north-eastern Anatolian plateau and Lesser Caucasus region where Neogene/Quaternary, Holocene volcanoes occur (Figure 6, 35 km depth). *Gök et al.* [2000] noted severe attenuation within the crust where the shear velocities were reduced at 90–100 km epicentral distances.

[28] While our preferred model does not fit the observed (stacked) receiver function exactly at each station, we suspect that the discrepancies are largely due to local lateral heterogeneities in the shallow crust and do not significantly affect the regional-scale velocity model, which is the primary objective of this study. The velocities and depths roughly resemble the crustal models based on Soviet era refraction profiles. The depths from the refraction models are approximate as the original figures were relatively low resolution and may have had geographic locations misplaced. *Kondorskaya et al.* [1981] reported Moho depths of 45–50 km in the Lesser Caucasus, 40–45 km in the Kura basin, and 50–55 km under the Greater Caucasus. The north-south refraction profile clearly showed low *P* velocities in the upper crust (~0–10 km) of the Kura basin overlying anomalously higher velocities in the lower crust, which closely matches the spatial distribution in Figure 6 at depths of 10 and 35 km. *Khalilov et al.* [1987] indicated Moho depths of ~56 km between the Caspian and the Black Sea with a granitic layer that ends at the South Caspian border. More recently, *Mangino and Priestley* [1998] used receiver functions at a site near station LKR to infer a Moho depth of 35 km. Our Moho depth at LKR is 42 km and we speculate that the thick sediments and substantial lateral velocity changes over a short distance at the edge of the South Caspian Basin may be the cause of the difference. The overall crustal structure of low-velocity upper crust over a higher-velocity lower crust is similar between the two models.

[29] Upper mantle velocities are low below most of the Anatolian plateau and extend north toward the Western Greater Caucasus but increase significantly toward the South Caspian Basin. The refraction results indicate a similar pattern for upper mantle *P* velocities but were slightly higher. *Hearn and Ni* [1994] observed very low *Pn* velocities below the Anatolian plateau and Caucasus, which matches the results shown here.

[30] The difference in velocities for the individual Love and Rayleigh inversions are shown at 57 and 85 km depth, where the lithospheric mantle is present the vertically polarized S wave travels faster than the horizontally polarized S wave (SV > SH). This feature is observed in the Greater Caucasus and Kura but not observed under the

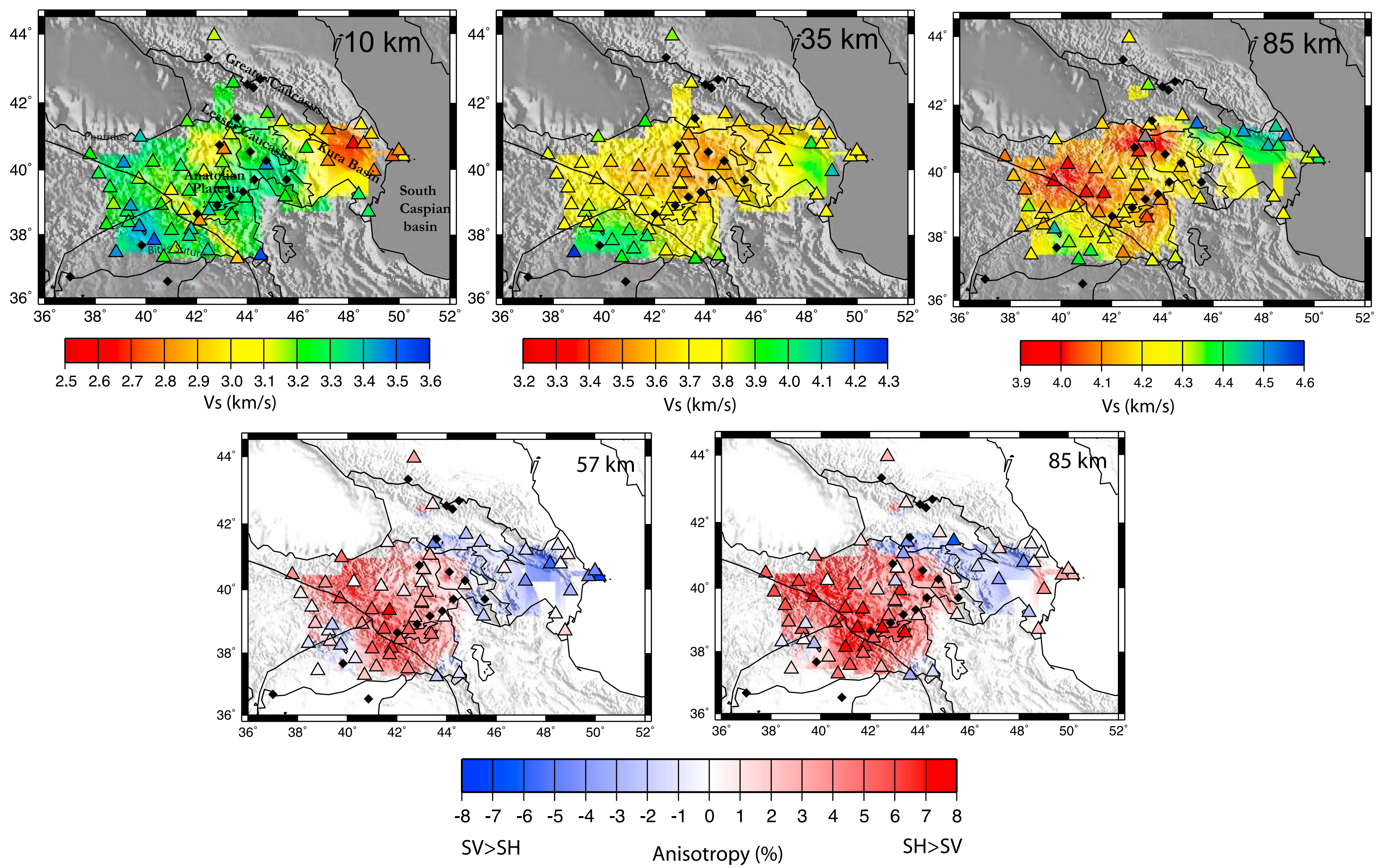

Figure 6. (top) Horizontal slices of velocities at upper crust (10 km), lower crust (35 km), and upper mantle (85 km). Small black diamonds show locations of Holocene volcanics. Thick sediments of Kura basin are still prominent at 10 km depth. Slowest velocities within the lower crust and upper mantle are observed in northeastern Arabian plateau and Lesser Caucasus. The lower crust in the Kura basin is relatively fast. (bottom) Maps showing anisotropies at 57 and 85 km depth.

Anatolian plateau and Lesser Caucasus between the depths of 57–100 km (Figure 6). We observe slower *S* wave velocities throughout the plateau, northern Arabian plate, Lesser Caucasus as well as SH being higher (4–8%) than SV. SH > SV in the asthenosphere might be related to the shear flow with a significant horizontal component. If it is the case we might consider this as the boundary of lithosphere. The lithosphere is possibly slightly thicker in Greater Caucasus, Kura basin (see the boundary in Figure 6).

[31] An additional and indirect test of the results is provided by observing regional wave propagation. Regional waves propagating in the crust (*Lg*) are sensitive to crustal thickness variations and in the upper mantle (*Sn*) are greatly affected by the upper mantle temperature variations. The presence of *Sn* is an indication of a stable and relatively thick lithospheric mantle. To test the validity of our velocity model we inspected regional waveforms by simply checking for the presence of *Sn* and *Lg*. We show an example, a magnitude 5.1 event that occurred in the northern part of Greater Caucasus recorded by most of our stations (Figure 7a). We show paths from event to station if *Sn* is present and was clearly observed within the 0.5–8 Hz passband. Both *Lg* and *Sn* completely disappear when they travel through the Anatolian plateau. Within Kura and part of the Greater Caucasus, *Sn* is a very prominent phase. We used the visually inspected waveforms following the technique of *Sandvol et al.* [2001] for an *Sn* efficiency tomography map. We added our observations to the existing data sets of *Sandvol et al.* [2001] and *Gök et al.* [2000, 2003]. *Sn* attenuation tomography is an objective approach for mapping *Sn* blockage zones. Discrete wave propagation efficiencies are used to obtain the inverse extinction path length for the parameterization; Figure 7b shows our *Sn* propagation efficiency map of the region. The region with very low *S* wave velocities (dotted in Figure 7b) at 85 km and significant seismic transverse anisotropy (SH > SV) generally coincides with the zones of inefficient *Sn* propagation.

[32] We also observe possible crustal melt zones with extremely low velocities in the mid to lower crust in easternmost Anatolia and the western Lesser Caucasus (Figure 6, 35 km slice). Overall this zone seems to coincide with the location of active volcanism but thinner crust. This suggest that these low velocities and possible crustal melt zones are produced from heating associated with a thin to absent mantle lid as opposed to the accumulation of large amounts of radiogenic material in a thickened crust. This is also consistent with the lack of crustal thickening that we observe in the eastern Anatolian plateau. On the basis of the mantle velocities, the thin lithosphere is limited to eastern Anatolia and does not extend into the Lesser Caucasus, Kura basin, or Greater Caucasus. This is consistent with the idea of a slab-break-off or delamination event occurring close to the Arabian-Eurasian plate boundary. However, the lack of crustal thickening in the regions of thinner lithosphere seems to argue for slab break off rather than delamination unlike other regions [*Seber et al.*, 1996].

[33] In the Kura basin and along the southern edge of the Greater Caucasus, the tectonic interpretation is not as clear. The low velocities in the upper crust are due to sediments which extend and thicken to the east into the South Caspian Basin. More striking is the lateral increase in lower crust and upper mantle velocities from the Lesser Caucasus to the Kura basin which is clearly evident as deep as 85 km (Figure 6). This indicates that the Kura basin fundamentally differs from the Lesser Caucasus. In some ways the Kura basin crust may resemble the crust underlying the South Caspian Basin but with a more continental affinity. However, at the western end of the Kura upper mantle velocities increase again toward the Black Sea and these increased velocities may exist under the Western Greater Caucasus as well, as suggested by our results as well as Holocene volcanism. Gravity data, as interpreted by *Ruppel and McNutt* [1990], also suggest a weak, hot and thermally altered lithosphere under the western Greater Caucasus as opposed to a more elastic and cold lithosphere in the eastern Greater Caucasus. While the major crustal structures (e.g., Greater Caucasus/Lesser Caucasus) run approximately east-west, it appears that the upper mantle varies significantly from the Caspian side to the Black Sea side.

7. Conclusions

[34] A comprehensive and unified shear wave velocity model based on joint inversion of receiver functions and surface waves has been developed for the Anatolian plateau-Caucasus region. Using data from 31 new stations combined with GSN data and a previous deployment, the shear wave structure of the crust and upper mantle has been estimated to a depth of 100 km. Low upper mantle shear velocities and *Sn* attenuation suggest elevated temperatures under the Anatolian plateau and extending northward to the western Greater Caucasus. To the east, upper mantle velocities increase under the Kura basin and eastern Greater Caucasus. The lithosphere structure varies considerably from the west to east between the Black Sea and South Caspian Basin.

[35] A full discussion of the tectonic implications of these results is beyond the scope of this paper but we present some preliminary observations. Crustal thickness patterns suggest the majority of crustal thickening has occurred far from the Arabian-Eurasian plate boundary along the Pontides and Greater Caucasus. This first suggests that there has been limited crustal thickening except in the northern portion of the collisional belt between Arabia and Eurasia. This thickening seems to have occurred against the strong rigid lithosphere of the Black Sea and Siberian craton that may have acted as a backstop to the weaker lithosphere of the Anatolian plateau and Lesser Caucasus. Given the low crustal shear velocities and the pervasive volcanism in the Eurasian crust just north of the Bitlis suture it seems unlikely that this was accomplished by transmitting stress from the plate boundary to the northern Pontides and Greater Caucasus. This crustal thickening might have occurred during the last stages of subduction of the NeoTethys when there was possibly a flat slab subduction below the Anatolian plateau [*Barazangi et al.*, 2006]. This would also be consistent with the idea that there was only significant crustal shortening prior to the development of continental escape and the associate northern and eastern Anatolian fault zones.

[36] The detailed crustal structure is poorly resolved with the current spatial distribution of stations but it is clear, on the basis of the variations in receiver functions between neighboring stations, that considerable spatial complexity in crustal structure exists, especially in the Greater Caucasus-Kura-South Caspian region. Resolving this complexity and understanding the underlying tectonics will require a denser distribution of stations.

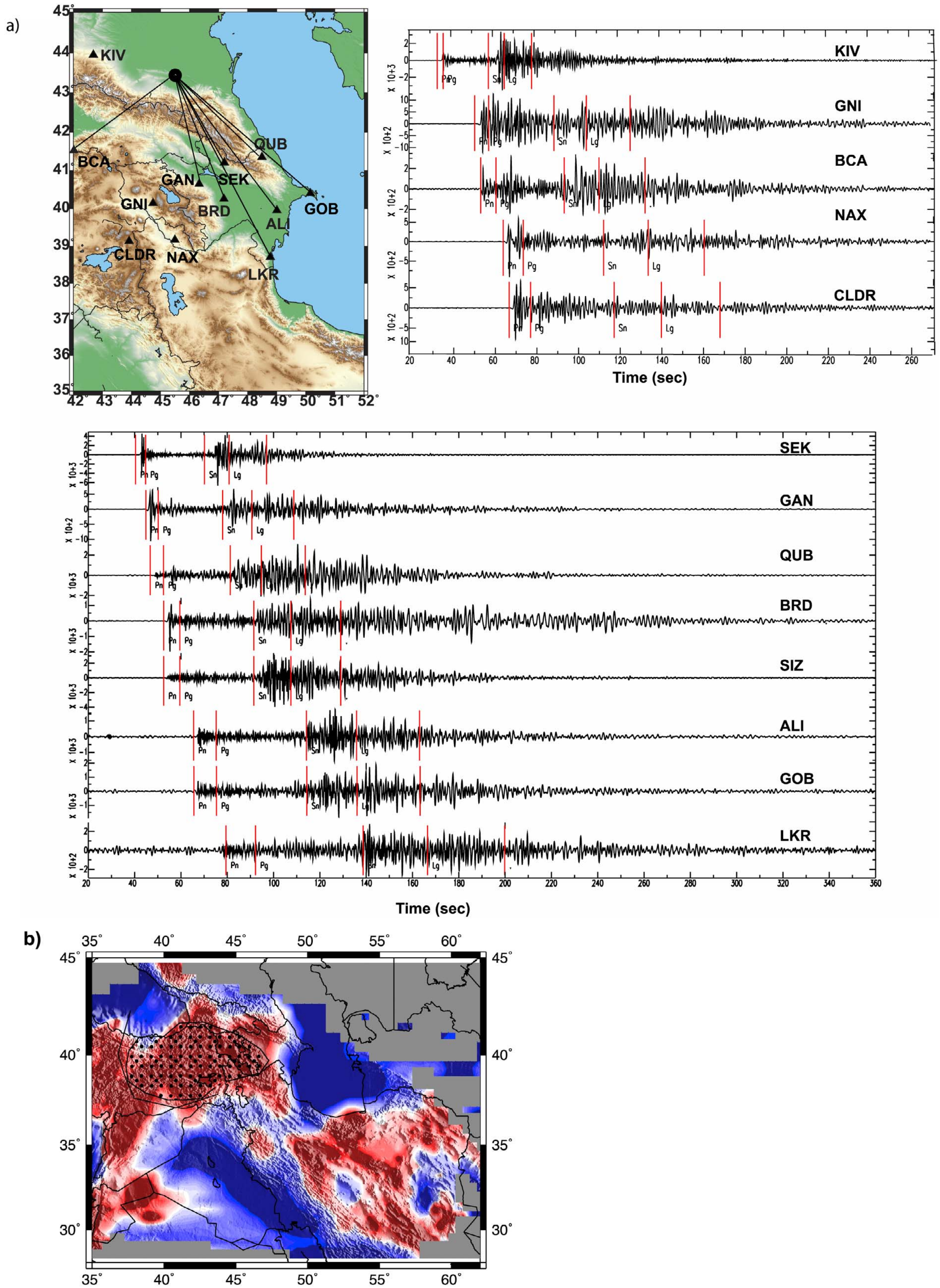

Figure 7. (a) An example event showing the propagation efficiencies of *Sn* and *Lg*. (b) *Sn* propagation efficiency tomography. Red is blocked *Sn*, and blue is efficiently propagating *Sn*. The shaded area is the low-velocity anomaly at 85 km (Figure 6).

[37] **Acknowledgments.** We would like to thank our Turkish, Azeri, and Georgian collaborators for their hospitality during our trips to the region. We would like to thank Rob Reilinger and Keith Priestley for discussions about the region. Special thanks to Nancy McGee for her insightful contribution. This project is funded by Air Force Research Laboratory contract FA8718-07-C-0007 to San Diego State University. This project was supported by the Lawrence Livermore National Laboratory under the auspices of the U.S. Department of Energy under contract DE-AC52-07NA27344. This is LLNL contribution LLNL-JRNL-468943.

References

Al-Lazki, A. I., D. Seber, E. Sandvol, N. Turkelli, R. Mohamad, and M. Barazangi (2003), Tomographic Pn velocity and anisotropy structure beneath the Anatolian plateau (eastern Turkey) and the surrounding regions, *Geophys. Res. Lett.*, *30*(24), 8043, doi:10.1029/2003GL017391.

Al-Lazki, A. I., E. Sandvol, D. Seber, M. Barazangi, N. Turkelli, and R. Mohamad (2004), On tomographic imaging of mantle lid velocity and anisotropy at the junction of the Arabian, Eurasian and African Plates, *Geophys. J. Int.*, *158*, 1024–1040, doi:10.1111/j.1365-246X.2004.02355.x.

Allen, M. B., S. Jones, A. Ismail-Zadeh, M. Simmons, and L. Anderson (2002), Onset of subduction as the cause of rapid Pliocene-Quaternary subsidence in the South Caspian Basin, *Geology*, *30*, 775–778, doi:10.1130/0091-7613(2002)030<0775:OOSATC>2.0.CO;2.

Allen, M., J. Jackson, and R. Walker (2004), Late Cenozoic reorganization of the Arabia-Eurasia collision and the comparison of short-term and long-term deformation rates, *Tectonics*, *23*, TC2008, doi:10.1029/2003TC001530.

Angus, D. A., D. C. Wilson, E. Sandvol, and J. F. Ni (2006), Lithospheric structure of the Arabian and Eurasian collision zone in eastern Turkey from S-wave receiver functions, *Geophys. J. Int.*, *166*, 1335–1346, doi:10.1111/j.1365-246X.2006.03070.x.

Barazangi, M., E. Sandvol, and D. Seber (2006), Structure and tectonic evolution of the Anatolian plateau in eastern Turkey, *GSA Today*, *409*, 463–473.

Bensen, G. D., M. H. Ritzwoller, M. P. Barmin, A. L. Levshin, F. Lin, M. P. Moschetti, N. M. Shapiro, and Y. Yang (2007), Processing seismic ambient noise data to obtain reliable broad-band surface wave dispersion measurements, *Geophys. J. Int.*, *169*, 1239–1260, doi:10.1111/j.1365-246X.2007.03374.x.

Bijwaard, H., W. Spakman, and E. R. Engdahl (1998), Closing the gap between regional and global travel time tomography, *J. Geophys. Res.*, *103*, 30,055–30,078, doi:10.1029/98JB02467.

Brunet, M. F., M. V. Korotaev, A. V. Ershov, and A. M. Nikishin (2003), The South Caspian Basin: A review of its evolution from subsidence modeling, *Sediment. Geol.*, *156*(1–4), 119–148, doi:10.1016/S0037-0738(02)00285-3.

Dewey, J. F., and A. M. C. Şengör (1979), Aegean and surrounding regions: Complex and multiplate continuum tectonics in a convergent zone, *Geol. Soc. Am. Bull.*, *90*, 84–92, doi:10.1130/0016-7606(1979)90<84:AASRCM>2.0.CO;2.

Ershov, A. V., and A. M. Nikishin (2004), Recent geodynamics of the Caucasus-Arabia-East Africa region, Geotectonics, *Engl. Transl.*, *38*, 123–136.

Göğüş, O. H., and R. N. Pysklywec (2008), Mantle lithosphere delamination driving plateau uplift and synconvergent extension in eastern Anatolia, *Geology*, *36*, 723–726, doi:10.1130/G24982A.1.

Gök, R., N. Turkelli, E. Sandvol, D. Seber, and M. Barazangi (2000), Regional wave propagation in Turkey and surrounding regions, *Geophys. Res. Lett.*, *27*, 429–432, doi:10.1029/1999GL008375.

Gök, R., E. Sandvol, N. Türkelli, D. Seber, and M. Barazangi (2003), *Sn* attenuation in the Anatolian and Iranian plateau and surrounding regions, *Geophys. Res. Lett.*, *30*(24), 8042, doi:10.1029/2003GL018020.

Gök, R., M. E. Pasyanos, and E. Zor (2007), Lithospheric structure of the continent-continent collision zone: Eastern Turkey, *Geophys. J. Int.*, *169*, 1079–1088, doi:10.1111/j.1365-246X.2006.03288.x.

Hearn, T., and J. Ni (1994), *Pn* velocities beneath continental collision zones: The Turkish-Iranian plateau, *Geophys. J. Int.*, *117*, 273–283, doi:10.1111/j.1365-246X.1994.tb03931.x.

Herrmann, R. B. (1973), Some aspects of band-pass filtering of surface waves, *Bull. Seismol. Soc. Am.*, *63*, 663–671.

Jackson, J., K. Priestley, M. Allen, and M. Berberian (2002), Active tectonics of the South Caspian Basin, *Geophys. J. Int.*, *148*, 214–245, doi:10.1046/j.1365-246X.2002.01588.x.

Julia, J., C. Ammon, R. Herrman, and A. Correig (2000), Joint inversion of receiver function and surface wave dispersion observations, *Geophys. J. Int.*, *143*, 99–112, doi:10.1046/j.1365-246x.2000.00217.x.

Julia, J., C. Ammon, and R. Herrmann (2003), Lithospheric structure of the Arabian Shield from the joint inversion of receiver functions and surface-wave group velocities, *Tectonophysics*, *371*, 1–21, doi:10.1016/S0040-1951(03)00196-3.

Kadinsky-Cade, K., M. Barazangi, J. Oliver, and B. Isacks (1981), Lateral variations of high-frequency seismic wave propagations at regional distances across the Turkish and Iranian plateaus, *J. Geophys. Res.*, *86*, 9377–9396, doi:10.1029/JB086iB10p09377.

Kadirov, F., and N. Askerhanova (1998), Gravity model of the Hekery-Rive-Fuzuli-Carli-Maraza (Azerbaijan) profile, paper presented at 60th EAGE Conference and Exhibition, Eur. Assoc. of Geosci. and Eng., Leipzig, Germany.

Khain, V. E. (2005), A possible factor responsible for the recent deepening of the Black and Caspian Seas and Caspian sea level fluctuations, *Dokl. Earth Sci.*, *403A*(6), 856–857.

Khain, V. E., and L. I. Lobkovskiy (1994), Relict seismicity in the Alpine belt of Eurasia mode of occurrence, *Geotectonics*, *Engl. Transl.*, *28*(3), 192–198.

Khalilov, E. N., S. F. Mekhtiev, and V. E. Khain (1987), On geophysical evidence supporting a collisional origin of the greater Caucasus, *Geotektonika*, *2*, 54–60.

Knapp, C. C., J. H. Knapp, and J. A. Connor (2004), Crustal-scale structure of the South Caspian Basin revealed by deep seismic reflection profiling, *Mar. Pet. Geol.*, *21*, 1073–1081, doi:10.1016/j.marpetgeo.2003.04.002.

Kondorskaya, N. V., et al. (1981), Joint analysis of seismological data by the USSP and DSS stations in the Caucasus region, *Pure Appl. Geophys.*, *119*, 1167–1179, doi:10.1007/BF00876695.

Ligorria, J. P., and C. J. Ammon (1999), Iterative deconvolution and receiver-function estimation, *Bull. Seismol. Soc. Am.*, *89*, 1395–1400.

Maggi, A., and K. Priestley (2005), Surface waveform tomography of the Turkish-Iranian Plateau, *Geophys. J. Int.*, *160*, 1068–1080, doi:10.1111/j.1365-246X.2005.02505.x.

Mangino, S., and K. Priestley (1998), The crustal structure of the southern Caspian region, *Geophys. J. Int.*, *133*, 630–648, doi:10.1046/j.1365-246X.1998.00520.x.

Martin, R., M. L. Krasovec, S. Romer, M. N. Toksöz, S. Kuleli, L. Gulen, and E. S. Vergino (2005), The Caucasus seismic information network study and its extension into Central Asia, paper presented at 27th Seismic Research Review: Ground-Based Nuclear Explosion Monitoring Technologies, Natl. Nucl. Secur. Admin., Rancho Mirage, Calif., 20–22 Sept.

Masson, F., Y. Djamour, S. Vangorp, J. Chéry, F. Tavakoli, M. Tatar, and H. Nankali (2006), Extension in NW Iran inferred from GPS enlightens the behavior of the south Caspian basin, *Earth Planet. Sci. Lett.*, *252*, 180–188, doi:10.1016/j.epsl.2006.09.038.

Nadirov, R. S., B. E. Bagirov, M. Tagiyevand, and I. Lerche (1997), Flexural plate subsidence, sedimentation rates, and structural development of the super-deep south Caspian Basin, *Tectonophysics*, *14*, 383–400.

Ozacar, A. A., H. Gilbert, and G. Zandt (2008), Upper mantle discontinuity structure beneath East Anatolian Plateau (Turkey) from receiver functions, *Earth Planet. Sci. Lett.*, *269*, 427–435, doi:10.1016/j.epsl.2008.02.036.

Pasyanos, M. E. (2005), A variable resolution surface wave dispersion study of Eurasia, North Africa, and surrounding regions, *J. Geophys. Res.*, *110*, B12301, doi:10.1029/2005JB003749.

Piromallo, C., and A. Morelli (2003), P wave tomography of the mantle under the Alpine-Mediterranean area, *J. Geophys. Res.*, *108*(B2), 2065, doi:10.1029/2002JB001757.

Priestley, K., C. Baker, and J. Jackson (1994), Implications of earthquake focal mechanism data for the active tectonics of the South Caspian Basin and surrounding regions, *Geophys. J. Int.*, *118*, 111–141, doi:10.1111/j.1365-246X.1994.tb04679.x.

Rebai, S., H. Philip, L. Dorbath, B. Borissoff, H. Haessler, and A. Cisternas (1993), Active tectonics in the Lesser Caucasus: Coexistence of compressive and extensional structures, *Tectonics*, *12*, 1089–1114, doi:10.1029/93TC00514.

Reilinger, R., et al. (2006), GPS constraints on continental deformation in the Africa-Arabia-Eurasia continental collision zone and implications for the dynamics of plate interactions, *J. Geophys. Res.*, *111*, B05411, doi:10.1029/2005JB004051.

Rodgers, A. J., J. F. Ni, and T. M. Hearn (1997), Propagation characteristics of short-period *Sn* and *Lg* in the Middle East, *Bull. Seismol. Soc. Am.*, *87*, 396–413.

Ruppel, C., and M. McNutt (1990), Regional compensation of the Greater Caucasus mountains based on an analysis of Bouguer gravity data, *Earth Planet. Sci. Lett.*, *98*, 360–379, doi:10.1016/0012-821X(90)90037-X.

Sandvol, E., D. Seber, A. Calvert, and M. Barazangi (1998), Grid search modeling of receiver functions: Implications for crustal structure in the Middle East and North Africa, *J. Geophys. Res.*, *103*, 26,899–26,917, doi:10.1029/98JB02238.

Sandvol, E., K. Al-Damegh, A. Calvert, D. Seber, M. Barazangi, R. Mohamad, R. Gök, N. Turkelli, and C. Gurbuz (2001), Tomographic imaging of *Lg* and

Sn propagation in the Middle East, *Pure Appl. Geophys.*, *158*, 1121–1163, doi:10.1007/PL00001218.
Sandvol, E., N. Turkelli, and M. Barazangi (2003), The Eastern Turkey Seismic Experiment: The study of a young continent-continent collision, *Geophys. Res. Lett.*, *30*(24), 8038, doi:10.1029/2003GL018912.
Seber, D., M. Barazangi, A. Ibenbrahim, and A. Demnati (1996), Geophysical evidence for lithospheric delamination beneath the Alboran Sea and Rif-Betic mountains, *Nature*, *379*, 785–790, doi:10.1038/379785a0.
Sengör, A. M. C. (1990), Plate tectonics and orogenic research after 25 years: A Tethyan perspective, *Earth Sci. Rev.*, *27*, 1–201, doi:10.1016/0012-8252(90)90002-D.
Sengör, A. M. C., S. Ozeren, T. Genc, and E. Zor (2003), East Anatolian high plateau as a mantle-supported, north-south shortened domal structure, *Geophys. Res. Lett.*, *30*(24), 8045, doi:10.1029/2003GL017858.
Shapiro, N. M., and M. Campillo (2004), Emergence of broadband Rayleigh waves from correlations of the ambient seismic noise, *Geophys. Res. Lett.*, *31*, L07614, doi:10.1029/2004GL019491.
Skobeltsyn, G. A., R. Mellors, R. Gök, N. Turkelli, G. Yetirmishli, and E. Sandvol (2009), Three dimensional S-wave velocity structure of the Caucasus region, *Seismol. Res. Lett.*, *80*, 346.
Toksöz, M., Y. Sun, C. Li, R. van der Hilst, and D. Kalafat (2006), Seismic tomography of the Arabian-Eurasian collision zone and tectonic implications, *Eos Trans. AGU*, *89*(53), Fall Meet. Suppl., Abstract T23D-01.
Türkoğlu, E., M. Unsworth, Ý. Çağlar, V. Tuncer, and Ü. Avşar (2008), Lithospheric structure of the Arabia-Eurasia collision zone in eastern Anatolia: Magnetotelluric evidence for widespread weakening by fluids?, *Geology*, *36*, 619–622, doi:10.1130/G24683A.1.
Vernant, P., and J. Chery (2006), Low fault friction in Iran implies localized deformation for the Arabia-Eurasia collision zone, *Earth Planet. Sci. Lett.*, *246*, 197–206, doi:10.1016/j.epsl.2006.04.021.
Wessel, P., and W. H. F. Smith (1998), New, improved version of generic mapping tools released, *Eos Trans. AGU*, *79*(47), 579, doi:10.1029/98EO00426.
Yang, Y., and D. W. Forsyth (2006), Regional tomographic inversion of amplitude and phase of Rayleigh waves with 2-D sensitivity kernels, *Geophys. J. Int.*, *166*, 1148–1160, doi:10.1111/j.1365-246X.2006.02972.x.
Zhu, L., and H. Kanamori (2000), Moho depth variation in southern California from teleseismic receiver functions, *J. Geophys. Res.*, *105*, 2969–2980, doi:10.1029/1999JB900322.
Zor, E., E. Sandvol, C. Gürbüz, N. Türkelli, D. Seber, and M. Barazangi (2003), The crustal structure of the East Anatolian plateau (Turkey) from receiver functions, *Geophys. Res. Lett.*, *30*(24), 8044, doi:10.1029/2003GL018192.

T. Godoladze and Z. Javakishvirli, Earth Research Institute, Ilia State University, 77 Nutsubidze str., Tbilisi, 0177, Georgia.

R. Gök, T. Hauk, R. J. Mellors, and M. Pasyanos, Lawrence Livermore National Laboratory, 7000 E. Ave., Livermore, CA 94550, USA. (gok1@llnl.gov)

E. Sandvol, Department of Geological Sciences, University of Missouri, Columbia, MO 65201, USA.

R. Takedatsu, Department of Geological Sciences, San Diego State University, San Diego, CA 92182, USA.

U. Teoman and N. Turkelli, Kandilli Observatory and Earthquake Research Institute, Department of Geophysics, Bogazici University, Istanbul 34684, Turkey.

G. Yetirmishli, Republic Seismic Survey Center, 13 Dr. Etibar Garaveliyev, Baku AZ1001, Azerbaijan.